Restoring cellular energetics promotes axon regeneration and functional recovery after spinal cord injury

Qi Han[1], Yuxiang Xie[2], Josue D. Ordaz[1], Andrew J. Huh[1], Ning Huang[2], Wei Wu[1], Naikui Liu[1], Kelly A. Chamberlain[2], Zu-Hang Sheng[2,3,*], Xiao-Ming Xu[1,*]

[1]Spinal Cord and Brain Injury Research Group, Stark Neurosciences Research Institute, Department of Neurological Surgery, Indiana University School of Medicine, Indianapolis, IN 46202, USA

[2]Synaptic Function Section, The Porter Neuroscience Research Center, National Institute of Neurological Disorders and Stroke, National Institutes of Health, Bethesda, MD 20892, USA

[3]Lead Contact: Z-H. Sheng (shengz@ninds.nih.gov)

*Correspondence: shengz@ninds.nih.gov (Z-H.S.), xu26@iupui.edu (X-M.X.)

Supplementary Figures 1-6

Figure S1 (Han et al)

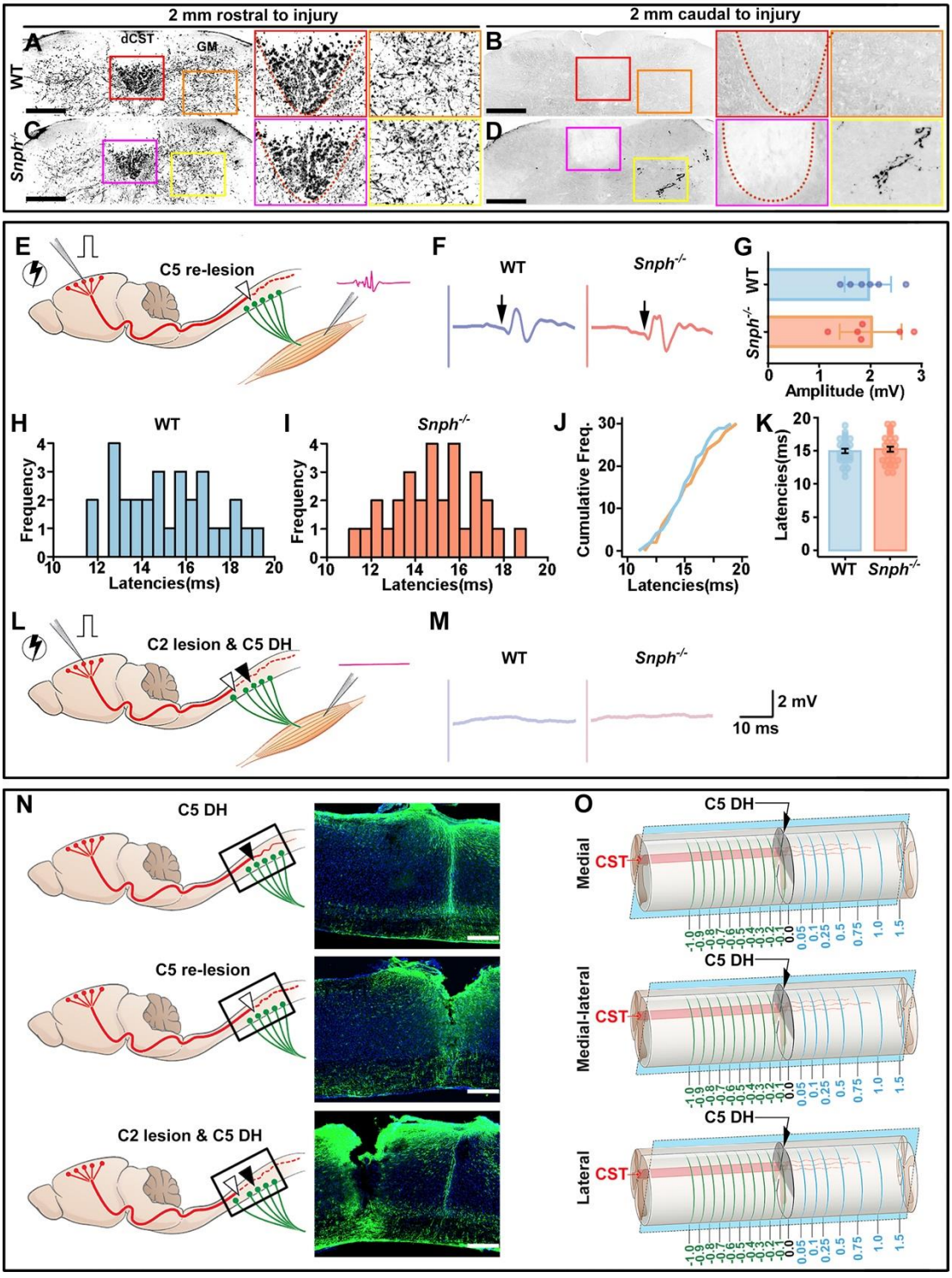

Figure S1 (Related to Figures 1 and 2). **The CST Regeneration in *Snph*$^{-/-}$ Mice Contributes to Cortico-Motoneuron Connections**

(A-D) Representative images show BDA-labeled CST axons in transverse sections at 2 mm rostral and 2 mm caudal to the C5 DH in WT and *Snph*$^{-/-}$ mice. Right panels: magnification of boxed area in left panel. Scale bars: 500 μm.

(E-K) The increased EMG responses in *Snph*$^{-/-}$ mice was abolished after the C5 re-lesion. Schematic diagram (E) illustrates the EMG recording in contralateral biceps in response to single-pulse stimulations in the motor cortex in mice after the C5 re-lesion. The sample EMG traces from WT (blue) and *Snph*$^{-/-}$ mice (red) are shown after the C5 re-lesion (F). The arrows indicate EMG onsets. (G) The averaged peak-to-peak EMG amplitude in WT (n = 6) and *Snph*$^{-/-}$ (n = 6) mice after the C5 re-lesion. (H, I) Frequency distributions of EMG latencies from WT and *Snph*$^{-/-}$ mice after C5 re-lesion. (J) A cumulative frequency distribution plot. Blue line, WT mice; red line, *Snph*$^{-/-}$ mice. (K) EMG latencies after single-pulse stimulation in the motor cortex in WT (14.95 ± 0.34, n = 30 stimulation sites from 6 mice) and *Snph*$^{-/-}$ mice (15.24 ± 0.39, n = 30 stimulation sites from 6 mice) after the C5 re-lesion.

(L, M) Acute C2 DH abolished EMG activity in *Snph*$^{-/-}$ mice. The schematic diagram shows EMG recording in contralateral biceps in response to single-pulse stimulations in the motor cortex after a second C2 lesion rostral to the C5 DH in mice (L).

(N) Illustrations of the lesion sites at the C5 DH (top panel, black arrowhead), C5 re-lesion at the same site (middle panel, white arrowhead), and C2 lesion rostral to the C5 lesion (bottom panel, white arrowhead). Representative images show each lesion site corresponding to the illustrations. The lesion sites were defined by reactive astrogliosis (GFAP-labeled, green) counterstained with DAPI (a nuclear dye, blue). Scale bars: 500 μm.

(O) Illustrations show parasagittal sections through three different spinal cord planes: medial, mediolateral, and lateral planes after the C5 DH (dark hemi-circle). The medial zone represents a cut through the dorsal and ventral funicular white matter and a small portion of the gray matter. The mediolateral zone represents a cut through the dorsal, intermediate and ventral gray matter. The lateral zone represents a cut through the dorsal and ventral gray matter with some lateral white matter.

Figure S2 (Han et al)

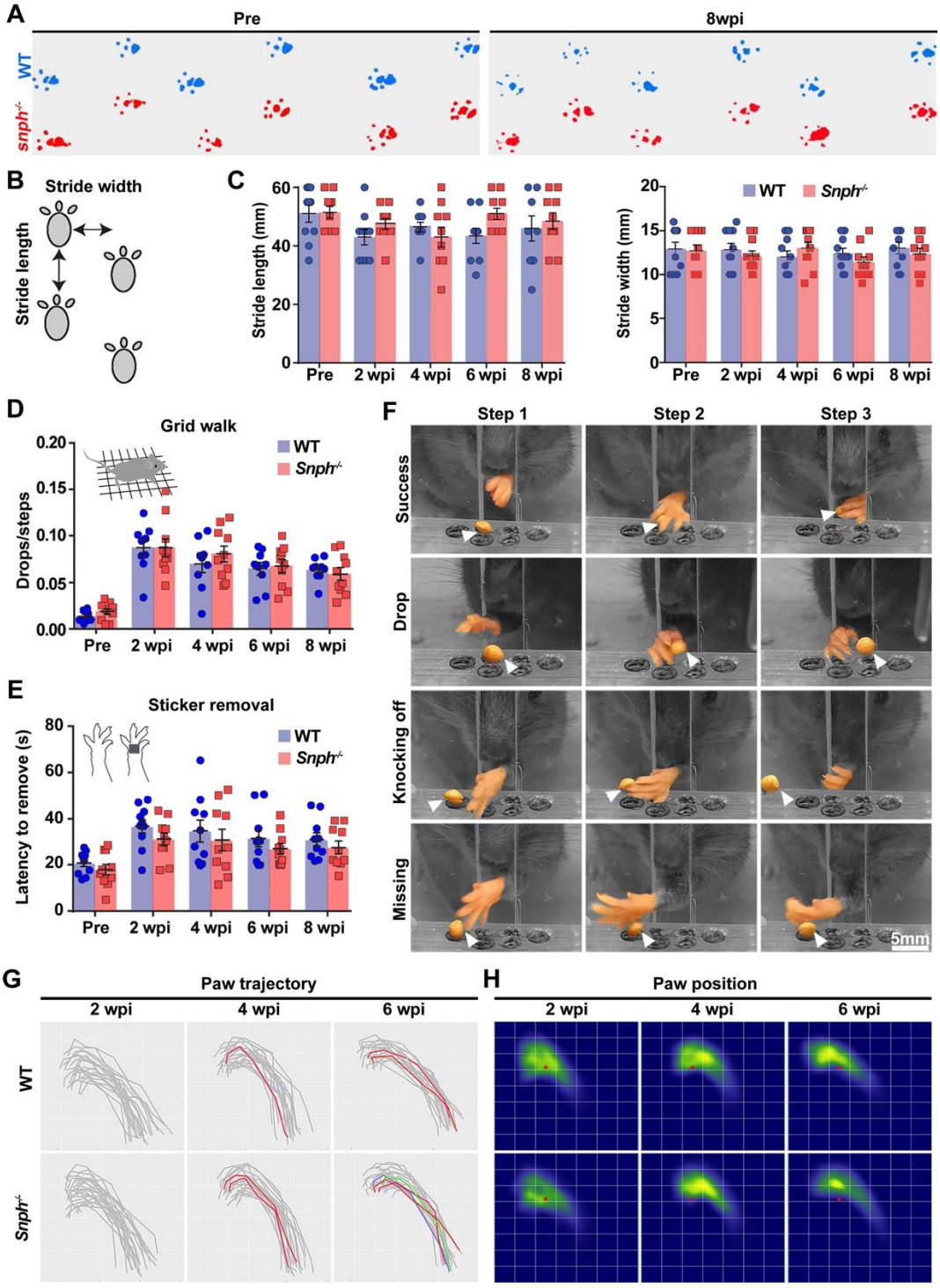

Figure S2 (Related to Figure 3). **Behavioral Assessments of WT and *Snph*$^{-/-}$ Mice Before and After C5 DH**

(A-C) Representative forepaw footprints in WT and *Snph*$^{-/-}$ mice measured before and after the C5 DH. The forepaws of WT mice were marked by blue ink and *Snph*$^{-/-}$ mice by red ink (A). A schematic drawing (B) and quantitative analysis (C) show the stride length and width before and after the C5 DH.

(D) An illustration of grid walking test (inset) and quantitative analysis of drop (error) rate show no significant differences between WT and *Snph*$^{-/-}$ mice in grid walking before and at 2-week intervals after the C5 DH up to 8 weeks post-injury (wpi).

(E) An illustration of sticker removal test (inset) and quantitative analysis show no significant differences in latency-to-remove the adhesive tape between WT and *Snph*$^{-/-}$ mice before and after C5 DH.

(F) Mouse reaching behaviors were observed and analyzed according to 2 categories: success and fail (including drop, missing or knocking off the food pellet). The performance was measured as success rate which is the percentage of successful reaches over the total number of reaching attempts. White arrows indicate food pellets.

(G) Paw trajectories during the reaching phase of the pellet retrievals in WT and *Snph*$^{-/-}$ mice from 2 to 6 weeks after the C5 DH. The successful reaches were colored and unsuccessful attempts were in grey.

(H) Paw location relative to the food pellet (red solid dot) during the grasping phase of the pellet retrieval in WT and *Snph*$^{-/-}$ mice from 2 to 6 weeks after the C5 DH.

Data were presented as mean ± sem. n = 10 per group (C, D, E). Two-way ANOVA with Bonferroni post hoc test.

Figure S3 (Han et al)

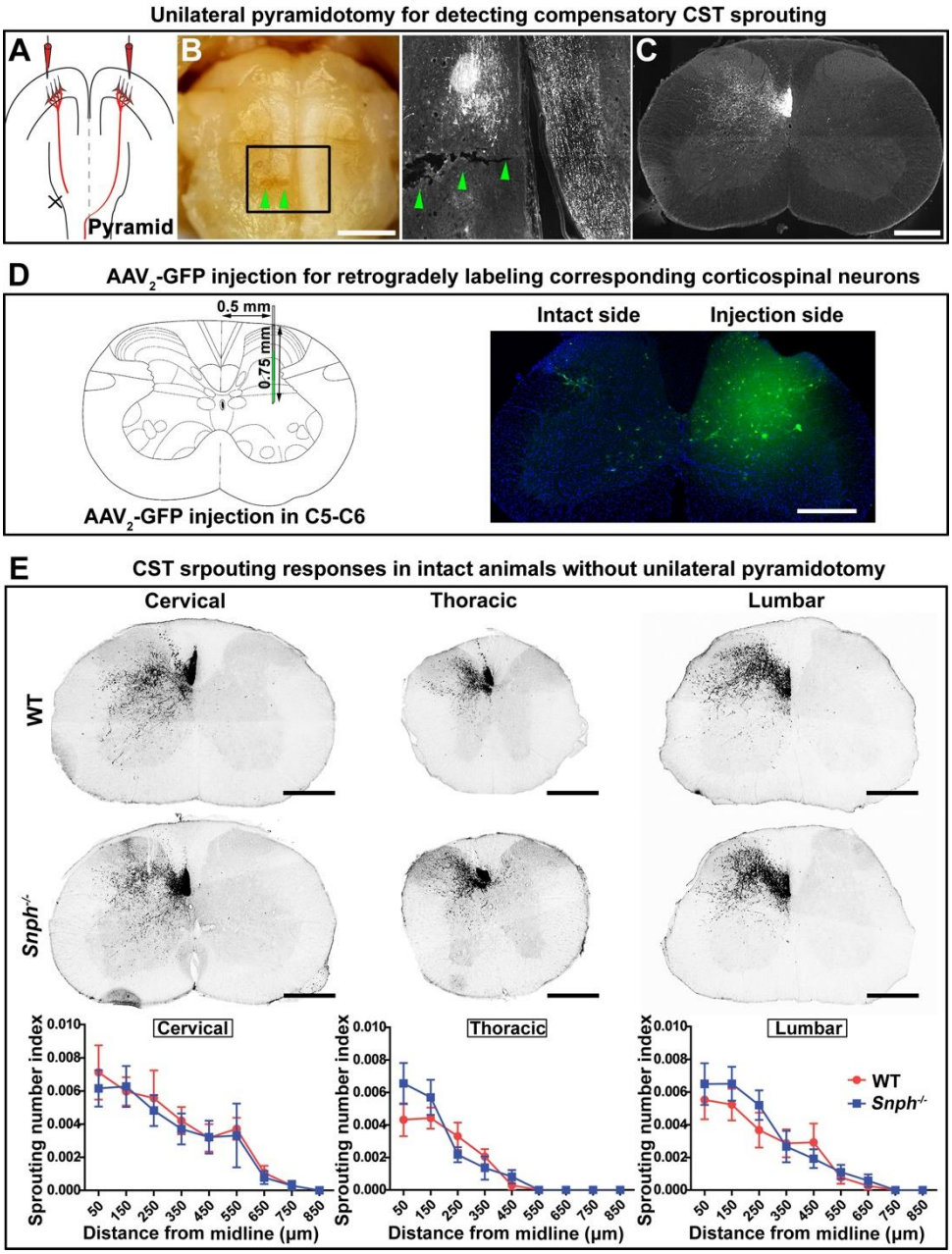

Figure S3 (Related to Figure 4). ***Snph*$^{-/-}$ Mice Display Minimal Cross-Midline Sprouting Without Unilateral Pyramidotomy**

(A-C) Diagram of a unilateral (left) pyramidotomy model. BDA injections were made into bilateral motor cortices (A). (B) Pyramidotomy (green arrowheads) is on the left side and a representative image in the horizontal section of the pyramid (boxed area in B) is on the right side, showing left-sided transection of the CST axons at lesion site (green arrows). BDA-labeled right-sided CST

axons were uninterrupted. (C) A representative image in a transverse section of the cervical spinal cord demonstrates the lack of descending CST main tract and its innervation in the gray matter on the contralesion side (right side) after a left-sided pyramidotomy (refers to A and B).

(D) Schematic diagram illustrates the reference coordinates of AAV_2-GFP injection into the C5-C6 level of the spinal cord to retrogradely label corticospinal neurons in layer V of the motor cortex. The representative image shows the confining of AAV_2-GFP injection to the denervated side of the spinal cord without spreading into the intact side of the CST.

(E) Representative images of the cervical, thoracic and lumbar spinal cord transverse sections show BDA-labeled CST axons in intact (left side) WT and *Snph*$^{-/-}$ mice without unilateral pyramidotomy. Quantification of trans-midline axons was counted at various distances from the midline in the cervical, thoracic, and lumbar spinal sections. Data were presented as mean ± sem. *n* = 4 mice per group. Five sections at each different region were quantified per mouse. Two-way ANOVA followed by Bonferroni post hoc test. Scale bars: 1 mm (B), 400 μm (C, D), 500 μm (E).

Figure S4 (Han et al)

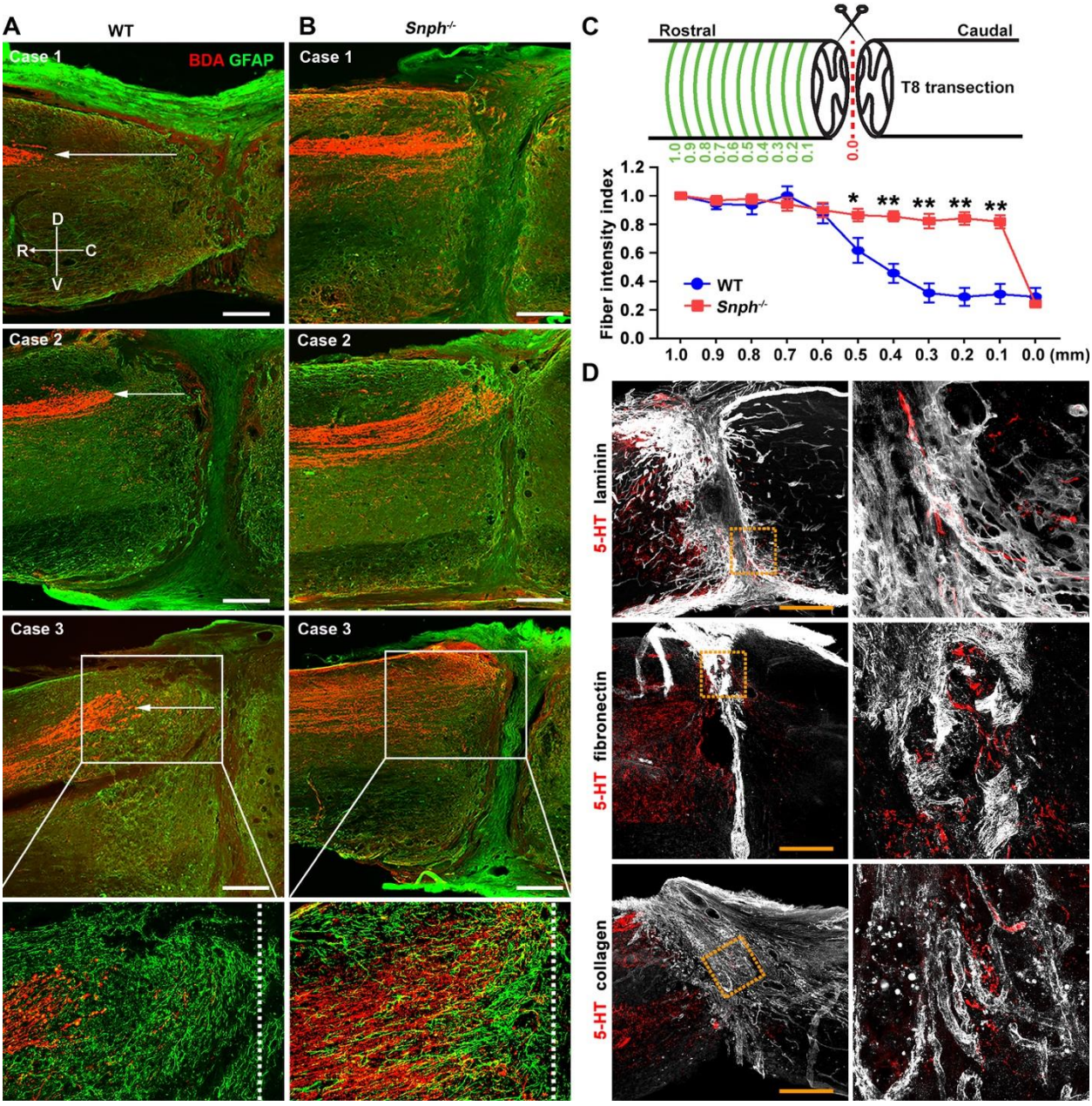

Figure S4 (Related to Figure 5). ***Snph*$^{-/-}$ Mice Do Not Display CST Axonal Retraction or Dieback after the T8 Spinal Complete Transection**

(A, B) Three different representative cases in WT (B) and *Snph*$^{-/-}$ (C) mice show the spatial relationship between BDA-labeled CST axons and the lesion center at 8 weeks after the T8 complete transection. Arrows indicate distances of CST axonal retraction from the rostral lesion border in WT mice (A). The lesion border was outlined by GFAP-labeled reactive astrogliosis. The

bottom images are high magnifications of boxed areas in Case 3 of both groups. The dash lines indicate rostral lesion edges. Compass: D, dorsal; V, ventral; R, rostral; C, caudal.

(C) The schematic diagram shows a complete spinal cord transection at T8. BDA-labeled CST axons were examined in cross-sections at various distances (green lines) from the lesion center (red dash line, 0.0 μm) up to 1.0 mm rostral to the injury. Quantification of BDA-labeled CST axon fiber intensity index at various distances from the lesion center. Data are presented as mean ± sem, n = 6 mice per group. Two-way ANOVA with Bonferroni post hoc test. * $P < 0.05$; ** $P < 0.01$.

(D) Representative images showing regenerated 5-HT-IR axons passing through the non-neuronal lesion cores and contacting multiple substrate molecules including laminin (upper), fibronectin (middle), and collagen (lower) following the complete transection. Right panels: high magnifications of boxed areas. Scale bars: 400 μm (A, B, D).

Figure S5 (Han et al)

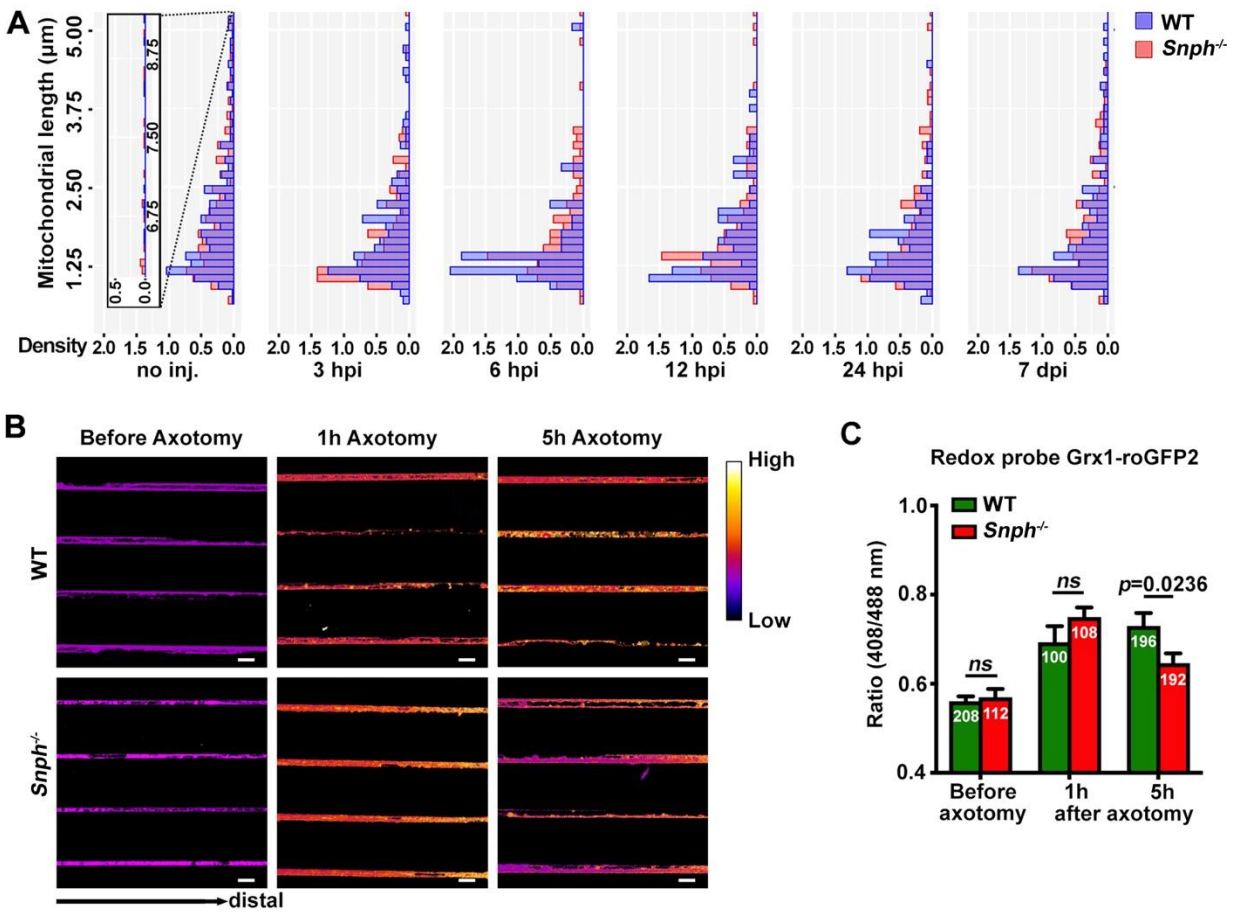

Figure S5 (Related to Figure 6). **Enhancing Mitochondrial Transport in *Snph*$^{-/-}$ Mice Benefits the Removal of ROS-related Toxicity in Injured Axons**

(A) Distribution of CMTMRos-labeled mitochondria length in WT (blue bar) and *Snph*$^{-/-}$ (red bar) mice. Data were obtained from non-injured control, 3, 6, 12, 24 hours, and 7 days after the C5 DH, *n* =3-4 mice per group per time point.

(B, C) Representative pseudo-color ratiometric images (B) and the 405/488nm ratiometric integrated intensity (C) of redox probe. Both WT and *Snph*$^{-/-}$ cortical neurons cultured in microfluidic chamber were infected with lentivirus expressing redox-sensitive Grx1-roGFP2 probe at DIV7, followed by imaging of distal 150-μm microgrooves before, 1 or 5 hours after axotomy at DIV12. Note that *Snph*$^{-/-}$ neurons showed declined redox level at 5 hours after injury when compared to WT neurons (P = 0.023). Data were analyzed from the total number of microgrooves indicated within bars from > 7 chambers in three experiments. Data were expressed as mean ± sem and analyzed by Student's *t* test. Scale bars, 10 μm.

Figure S6 (Han et al)

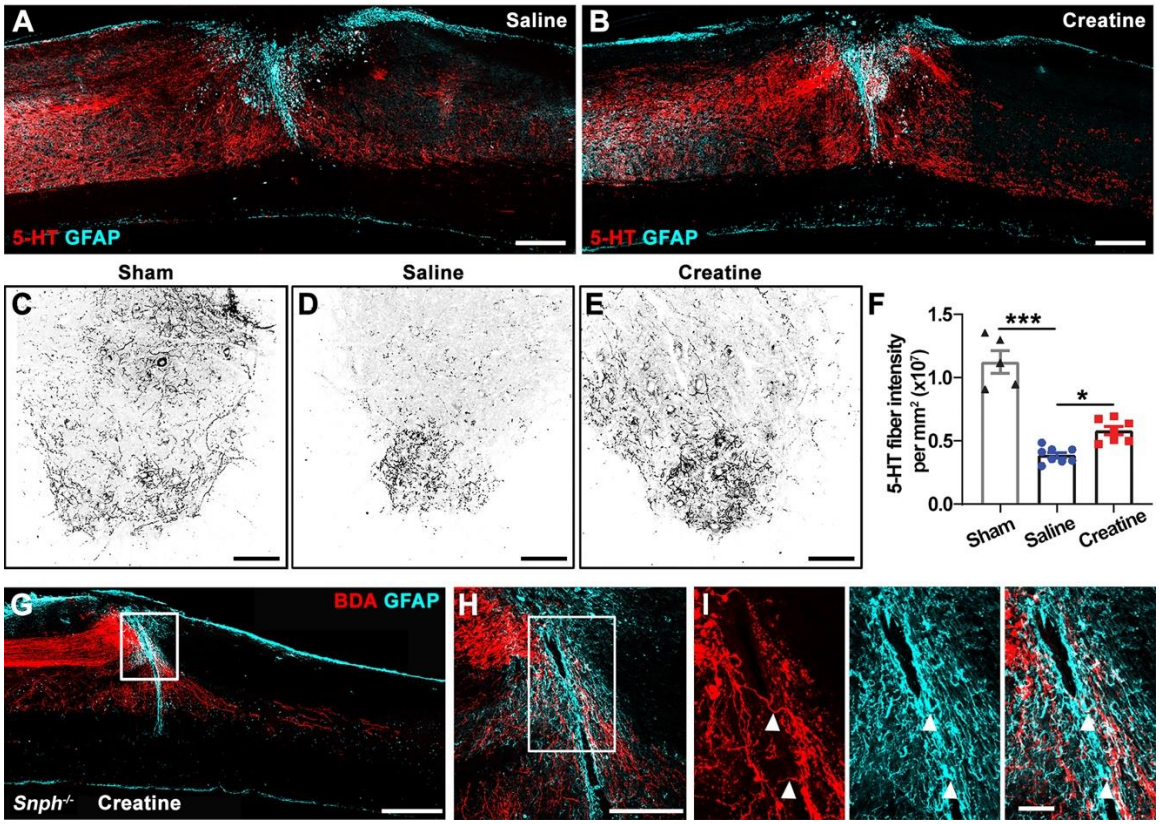

Figure S6 (Related to Figure 7). **Creatine Treatment Elevates Serotoninergic Axonal Regeneration After SCI**

(A, B) Representative images of double labeling for serotoninergic axons (5-HT) and reactive astrocytes (GFAP) in sagittal sections of *Snph*$^{-/-}$ mice treated with either saline or creatine at 8 wpi. Note that 5-HT-IR axons in both animal groups were present in the caudal spinal cord.

(C-F) Representative images from cross-sections from the sham control mice or the SCI mice treated with either saline or creatine at 4 mm caudal to the lesion at 8 wpi. 5-HT-IR fiber intensity was quantified from the ventral horn of spinal cord in each animal group (F). Data were presented as mean ± sem, n = 5-8 mice per group. One-way ANOVA with Tukey post hoc test. *$P < 0.05$; ***$P < 0.001$.

(G-I) Representative images of sagittal sections in *Snph*$^{-/-}$ mice with creatine treatment at 8 wpi. (H, I) High magnification image in boxed areas showing BDA-labeled regenerated CST axons along with GFAP positive astrocytes past the lesion site. Scale bars: 400 μm (A, B), 100 μm (C-E), 500 μm (G), 200 μm (H), 50 μm (I).